Article

Ternary Compounds in the Sn-Rich Section of the Ba–Ga–Sn System: Ba$_8$Ga$_{16-x}$Sn$_{30+x}$ (1.1 ≤ *x* ≤ 2.8) Clathrates of Type-I and Type-VIII, and BaGa$_{2-x}$Sn$_{4+x}$ (*x* ≈ 0.2) with a Clathrate-like Structure

Marion C. Schäfer [1], Yuki Yamasaki [1,2], Veronika Fritsch [3] and Svilen Bobev [1,]*

[1] Department of Chemistry and Biochemistry, University of Delaware, Newark, DE 19716, USA
[2] Department of Chemistry, Hosei University, Tokyo 194-0298, Japan
[3] Physikalisches Institut, Karlsruher Institut für Technologie, D-76131 Karlsruhe, Germany

* Author to whom correspondence should be addressed; E-Mail: bobev@udel.edu;
Tel.: +1-302-831-8720; Fax: +1-302-831-6335.

Abstract: Systematic syntheses in the Ba–Ga–Sn system confirmed the existence of a new ternary phase BaGa$_{1.79}$Sn$_{4.21(2)}$ (EuGa$_2$Ge$_4$ structure type; orthorhombic space group *Cmcm*, *Pearson* symbol *oS*28) with lattice parameters *a* = 4.5383(6) Å, *b* = 12.2486(16) Å, *c* = 14.3747(19) Å. The structure is best viewed as an open-framework based on tetrahedrally coordinated Sn/Ga atoms with Ba atoms enclosed in the voids within it. The new phase co-precipitates with two other compounds with very similar compositions—Ba$_8$Ga$_{14.5}$Sn$_{31.5(4)}$ (K$_4$Si$_{23}$ structure type; cubic space group $Pm\overline{3}n$, *Pearson* symbol *cP*54; *a* = 11.6800(12) Å), and Ba$_8$Ga$_{13.2}$Sn$_{32.8(3)}$, (Eu$_4$Ga$_8$Ge$_{15}$ structure type; cubic space group $I\overline{4}3m$, *Pearson* symbol *cI*54; *a* = 11.5843(7) Å). Detailed discussion on how syntheses affect the crystal chemistry, and the temperature dependence of the atomic displacement parameters, obtained from single-crystal structure refinements, are also reported in this article.

Keywords: clathrate type-I; clathrate type-VIII; barium; gallium; tin; crystal structure

1. Introduction

Clathrates based on Si, Ge, or Sn have been known for close to five decades already, but only recently, the interest in these compounds with rigid covalent networks has shifted towards their potential for optical, thermoelectric and other valuable applications [1-3]. Although theoretical calculations suggest thermodynamic stability for a variety of such open-frameworks, only several structures (referred to as type-I, -II, *etc.*) have been found thus far. Clathrate type-I, which is the most common of all, crystallizes in primitive cubic unit cell with 46 framework-building atoms per unit cell, which are all tetrahedrally coordinated. They form 24-atom polyhedra with twelve pentagonal and two hexagonal faces and smaller 20-atom pentagonal dodecahedra. These "voids" can accommodate alkali- and/or alkaline-earth metal atoms, and thus, the formula of the fully stoichiometric clathrate type-I is A_8Tt_{46}, where *A* represents the corresponding metal atoms and *Tt* stands for *Tetrel, i.e.,* group 14 elements, respectively. It has also been well established that the structure is amenable to modifications through substitution of *Tt*-atoms from the network with an electron-poorer element, from groups 13 or 12 for example, which allows for tunable properties [4]. This approach can be applied to all known clathrate types as well.

While the crystal chemistry and the chemical bonding in most of the clathrate structures are satisfactorily understood today, one major difficulty persists, and it is in the selective synthesis of each type. The reasons for that are very simple: *i*) the ratios of framework atoms to cavity atoms in all of the clathrates are remarkably close; *ii*) the relative thermodynamic stability of the known clathrate types is nearly the same. A possible solution to this synthetic problem can be based on the fact that the polyhedra in the clathrates' structures are of quite different dimensions. Implementation of this idea allows for the rational synthesis of the clathrate type-II compounds (Cs or Rb)$_8$Na$_{16}$(Si or Ge)$_{136}$ [5,6] and (Cs or Rb)$_8$Na$_{16}$(Ga,Si)$_{136}$ [7]—ratio of 24:136 or 1:5.67—instead of the analogous clathrates type-I compounds Na$_8$Si$_{46}$ [8] or Rb$_8$Ga$_8$Ge$_{38}$ [9]—ratio of 8:46 or 1:5.75—where the two cavities are closer in size.

A control over whether type-I or type-VIII clathrates are realized is subtler, as both have the same nominal composition and are typically considered as polymorphs [10-15]. It has already been shown for α- and β-Eu$_8$Ga$_{16}$Ge$_{30}$ [10] that the two forms can be interconverted via careful selection of the synthesis methods. Heat treatments have again been indicated to be the decisive factors as to which phase occurs with regard to Ba$_8$Ga$_{16}$Sn$_{30}$ (rather Ba$_8$Ga$_{16-x}$Sn$_{30+x}$, where $x \leq \pm2.8$) [11-15], however, in this instance, the type-I (previously known as β-form) [11,12] and the type-VIII (previously known as α-form) [12-15] clathrates, does not seem to "mirror" the dimorphism of the respective Eu$_8$Ga$_{16}$Ge$_{30}$ compounds [10].

With this paper, we report the results of our extensive work on type-I and type-VIII Ba$_8$Ga$_{16}$Sn$_{30}$ clathrates, which provide no evidence to support (ir)reversible $\alpha \leftrightarrow \beta$ phase transitions, suggesting they are better regarded as different, albeit closely related phases. We also further the knowledge on the phase-relationships in the Ba–Ga–Sn system, by reporting the novel ternary phase with a clathrate-like framework structure, BaGa$_2$Sn$_4$ (rather BaGa$_{2-x}$Sn$_{4+x}$, where $x \approx 0.2$), which is isotypic with EuGa$_2$Ge$_4$ [16-18]. BaGa$_{2-x}$Sn$_{4+x}$ is only the second ternary compound with this structure, after the archetype, and our structure refinements from X-ray single-crystal data provide, for a first time, a reliable data on the distribution of Ga and *Tt*-atoms on the framework sites.
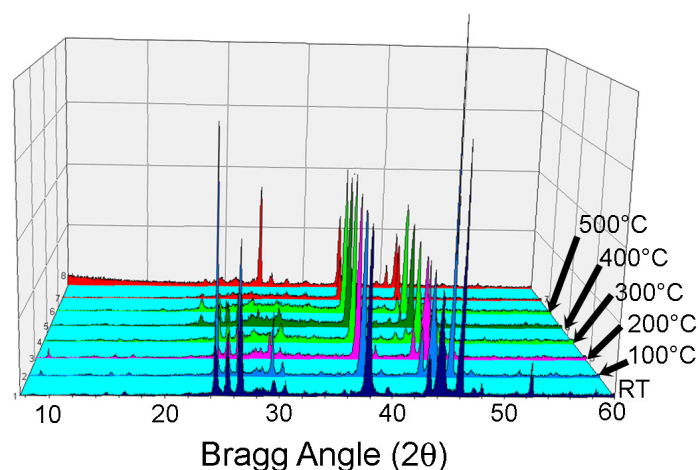
2. Results and Discussion

2.1. Synthesis and Thermal Analysis

In spite of the extensive prior experimental work in the system Ba–Ga–Sn [11-15,19-24], there remain some open questions, such as the existence of the only type-II clathrate with Sn, $Ba_{16}Ga_{32}Sn_{104}$ [25], and the proposed (but not proven) dimorphism of type-I and type-VIII $Ba_8Ga_{16}Sn_{30}$ clathrates [11-15]. Our systematic investigations, using both conventional solid-state synthesis methods, as well as molten fluxes have produced evidence for only three phases in the Sn-rich part of the phase diagram— type-I $Ba_8Ga_{16-x}Sn_{30+x}$ ($x \leq \pm1.5$) clathrate, type-VIII $Ba_8Ga_{16-x}Sn_{30+x}$ ($x \leq \pm2.8$) clathrate, and the new ternary phase $BaGa_{2-x}Sn_{4+x}$ ($x \approx 0.2$). The results from our exploratory work can be summarized as follows:

- type-I $Ba_8Ga_{16-x}Sn_{30+x}$ (previously known as β-form) clathrate is the major product of all stoichiometric or Sn flux reactions at high temperature, which are cooled quickly and annealed at temperatures below 450 °C before the removal of the flux;
- $BaGa_{2-x}Sn_{4+x}$ is the minor product of the above reactions and appears to always co-crystallize with the clathrate phase (note how close the nominal compositions are);
- type-VIII $Ba_8Ga_{16-x}Sn_{30+x}$ (previously known as α-form) clathrate is the major product of Sn of Sn/Ga flux reactions at low temperature, e.g., 500 °C;
- type-I $Ba_8Ga_{16-x}Sn_{30+x}$ clathrate readily forms via melting of stoichiometric mixtures of the elements at high-temperature, while type-VIII $Ba_8Ga_{16-x}Sn_{30+x}$ does not;
- when the Sn flux method is employed, reactions with the same ratios of Ba, Ga and Sn produce different phases if the flux is removed at 700 °C ($BaSn_3$ [26]) *vs* 400 °C (type-I $Ba_8Ga_{16-x}Sn_{30+x}$ clathrate).

In addition, thermal analysis of pure type-I $Ba_8Ga_{16-x}Sn_{30+x}$ clathrate suggests that it decomposes above 500 °C, confirming the DSC results reported by *Takabatake et al* [14,27]. However, temperature dependent *in-situ* powder X-ray diffraction reveals that the degradation of the sample begins at much lower temperature, ca. 300–350 °C (Figure 1). As seen from the figure, the material is significantly changed even below 300 °C and completely molten above *ca.* 500 °C; only Bragg peaks due to elemental Sn can be indexed upon cooling the melt to room temperature. Similar behavior is observed for the type-VIII $Ba_8Ga_{16-x}Sn_{30+x}$ clathrate with no signs of phase transitions neither in the calorimetry signals, nor in the *in-situ* powder X-ray diffraction pattern. The above indicates that the phase-relationships between type-I and type-VIII $Ba_8Ga_{16}Sn_{30}$ clathrates are different than those in the Eu–Ga–Ge counterparts. Apparently, both type-I and type-VIII $Ba_8Ga_{16}Sn_{30}$ clathrates decompose peritectically and cannot be transformed into each other (not at least under ambient pressure). Hence, we argue that the α- and β- designations are irrelevant, and referring to the type-VIII and type-I clathrates as low- and high-temperature forms, respectively, is unjust.

Figure 1. Temperature dependent *in-situ* powder X-ray diffraction patterns for type-I clathrate $Ba_8Ga_{14.5}Sn_{31.5(4)}$. The peak at ca. 39° 2θ that does not change with T is from the Pt thermocouple.

We also note that compared to the previously reported synthetic conditions [11-15] the reactions we have explored involve higher amounts of Sn (flux), and therefore our materials are a little different than those found in the literature, i.e., slightly Sn-richer. For example, the refined formula of our type-I clathrate is $Ba_8Ga_{14.5}Sn_{31.5(4)}$ vs $Ba_8Ga_{16.8}Sn_{29.2}$ [11] or $Ba_8Ga_{16.9}Sn_{29.1}$ [12]. Similarly, the refined formula of our type-VIII clathrate ($Ba_8Ga_{13.2}Sn_{32.8(3)}$) is also further away from the ideal $Ba_8Ga_{16}Sn_{30}$ composition and slightly Sn-richer than $Ba_8Ga_{17.4}Sn_{28.6}$ [13], $Ba_8Ga_{17.2}Sn_{28.8}$ [15] and $Ba_8Ga_{16.5}Sn_{29.5}$ [12].

2.2. Crystal Chemistry of Clathrate type-I

$Ba_8Ga_{14.5}Sn_{31.5(4)}$ with type-I structure crystallizes in the cubic space group $Pm\overline{3}n$ (no. 223, *Pearson* symbol *cP*54; Table 1 and 2) with a periodicity constant $a = 11.6800(12)$ Å at room temperature. This value is shorter than the reported unit cells for $Ba_8Ga_{16.8}Sn_{29.2}$ ($a = 11.744(2)$ Å) [11] and $Ba_8Ga_{15.2}Sn_{30.8}$ ($a = 11.708(1)$ Å) [12], which is somewhat unexpected given that our crystals are Sn-richer (*vide supra*) and that the Pauling's radius of Sn (1.42 Å) is larger than that of Ga (1.25 Å) [28]. The open-framework (Figure 2, *left*) is made of statistically disordered Ga and Sn atoms, located at three different *Wyckoff* sites—6*c*, 16*i* and 24*k*. The 46 framework sites (per unit cell) can be viewed as forming six larger $(Ga,Sn)_{24}$ tetrakaidecahedra and two smaller $(Ga,Sn)_{20}$ dodecahedra (in analogy with the fullerenes, the former can be denoted as $5^{12}6^2$, and the latter as 5^{12}, respectively). The tetrakaidecahedra share their hexagonal faces and create a system of three perpendicular and nonintersecting "channels" running along the axes of the cube. Smaller 20-atom pentagonal dodecahedra are enclosed between them. We point out here that although the framework is made of approximately 1/3 Ga and 2/3 Sn, the distribution of two elements is not uniform on the three sites. For example, the 6*c* site (Ga:Sn = 67:33) is preferentially occupied by Ga (Table 3), while the Sn atoms are primarily found at the 16*i* (Ga:Sn = 31:69) and 24*k* (Ga:Sn = 23:77) sites. Very similar site occupancies are observed in $Ba_8Ga_{16.8}Sn_{29.2}$ (Sn amount: 27%, 64% and 73%, respectively) [11] and in $Ba_8Ga_{16-x}Sn_{30+x}$ ($x \leq \pm 0.9$); 29–33%, 64–66% and 74–75%, respectively) [12]. *Iversen et al.* have

analyzed these traits in other clathrates and have suggested that the reason for the preferential (sometimes even exclusive) occurrence of the *Triel* over the *Tetrel* element at the 6*c* site is so that the unfavorable *Tr–Tr* contacts are minimized [3].

Table 1. Important crystal data and structure refinement parameters for $Ba_8Ga_{14.5}Sn_{31.5(4)}$ (clathrate type-I), $Ba_8Ga_{13.2}Sn_{32.8(3)}$ (clathrate type-VIII), and $BaGa_{1.79}Sn_{4.21(2)}$.

empirical formula	$Ba_8Ga_{14.5}Sn_{31.5(4)}$	$Ba_8Ga_{13.2}Sn_{32.8(3)}$	$BaGa_{1.79}Sn_{4.21(2)}$
Fw, g/mol	5853.58	5916.63	761.41
Crystal system	Cubic	Cubic	Orthorhombic
Space group	$Pm\bar{3}n$ (no. 223)	$I\bar{4}3m$ (no. 217)	$Cmcm$ (no. 63)
a (Å)	11.6800(12)	11.5843(7)	4.5383(6)
b (Å)			12.2486(16)
c (Å)			14.3747(19)
V (Å^3)	1593.41	1554.57	799.06
Z	1	1	4
T (K)	293(2)	293(2)	120(2)
Radiation, λ (Å)	Mo Kα, 0.71073	Mo Kα, 0.71073	Mo Kα, 0.71073
ρ (g·cm^{-3})	6.018	6.273	6.333
μ (cm^{-1})	229.8	234.9	236.2
R_1 [$I > 2\sigma(I)$][a]	0.030	0.019	0.031
wR_2 [$I > 2\sigma(I)$][a]	0.058	0.049	0.061
largest peak/hole (e$^-$·Å^{-3})	1.19/ –0.88	0.86/ –1.10	1.35/ –2.02

[a] $R_1 = \sum ||F_o| - |F_c||/\sum|F_o|$; $wR_2 = [\sum[w(F_o^2 - F_c^2)^2]/\sum[w(F_o^2)^2]]^{1/2}$, and $w = 1/[\sigma^2 F_o^2 + (A \cdot P)^2 + B \cdot P]$, $P = (F_o^2 + 2F_c^2)/3$; A and B are weight coefficients.

Table 2. Selected structure refinement parameters for $Ba_8Ga_{14.5}Sn_{31.5(4)}$ (clathrate type-I) in the temperature range 100–200 K.

T (K)	100(2)	125(2)	150(2)	175(2)	200(2)
a (Å)	11.6588(8)	11.6623(7)	11.6681(11)	11.6691(7)	11.6727(15)
μ (cm^{-1})	231.0	230.8	230.5	230.4	230.2
R_1 [$I > 2\sigma(I)$][a]	0.026	0.027	0.032	0.027	0.032
wR_2 [$I > 2\sigma(I)$][a]	0.052	0.057	0.063	0.054	0.068
largest peak/hole (e$^-$·Å^{-3})	0.80/ –0.88	1.09/ –1.03	1.02/ –1.46	0.90/ –0.93	0.98/ –0.93

[a] $R_1 = \sum ||F_o| - |F_c||/\sum|F_o|$; $wR_2 = [\sum[w(F_o^2 - F_c^2)^2]/\sum[w(F_o^2)^2]]^{1/2}$, and $w = 1/[\sigma^2 F_o^2 + (A \cdot P)^2 + B \cdot P]$, $P = (F_o^2 + 2F_c^2)/3$; A and B are weight coefficients.

Table 3. Atomic coordinates and isotropic displacement parameters $(U_{eq})^a$ for $Ba_8Ga_{14.5}Sn_{31.5(4)}$ (clathrate type-I) at variable temperature.

T (K)	Atom	Site	x	y	z	U_{eq} (Å^2)
	Ba1 [b]	24k	0	0.2533(9)	0.4600(3)	0.0359(12)
	Ba2	2a	0	0	0	0.0117(5)
100(2)	Sn1/Ga1 [c]	24k	0	0.31233(6)	0.11844(6)	0.0115(3)
	Sn2/Ga2 [d]	16i	0.18411(4)	0.18411(4)	0.18411(4)	0.0118(3)
	Sn3/Ga3 [e]	6c	$^1/_4$	0	$^1/_2$	0.0126(8)
	Ba1 [b]	24k	0	0.2553(9)	0.4612(3)	0.0373(14)
	Ba2	2a	0	0	0	0.0124(6)
125(2)	Sn1/Ga1 [c]	24k	0	0.31227(6)	0.11846(6)	0.0122(3)
	Sn2/Ga2 [d]	16i	0.18414(5)	0.18414(5)	0.18414(5)	0.0127(3)
	Sn3/Ga3 [e]	6c	$^1/_4$	0	$^1/_2$	0.0135(6)
	Ba1 [b]	24k	0	0.2534(11)	0.4606(3)	0.0391(19)
	Ba2	2a	0	0	0	0.0131(7)
150(2)	Sn1/Ga1 [c]	24k	0	0.31221(8)	0.11843(7)	0.0125(3)
	Sn2/Ga2 [d]	16i	0.18416(5)	0.18416(5)	0.18416(5)	0.0129(4)
	Sn3/Ga3 [e]	6c	$^1/_4$	0	$^1/_2$	0.0133(8)
	Ba1 [b]	24k	0	0.2549(10)	0.4619(3)	0.0408(15)
	Ba2	2a	0	0	0	0.0145(6)
175(2)	Sn1/Ga1 [c]	24k	0	0.31227(6)	0.11846(6)	0.0142(3)
	Sn2/Ga2 [d]	16i	0.18417(6)	0.18417(6)	0.18417(6)	0.0139(3)
	Sn3/Ga3 [e]	6c	$^1/_4$	0	$^1/_2$	0.0144(6)
	Ba1 [b]	24k	0	0.2532(18)	0.4623(4)	0.0481(21)
	Ba2	2a	0	0	0	0.0174(7)
200(2)	Sn1/Ga1 [c]	24k	0	0.31224(7)	0.11845(7)	0.0157(3)
	Sn2/Ga2 [d]	16i	0.18413(5)	0.18413(5)	0.18413(5)	0.0160(4)
	Sn3/Ga3 [e]	6c	$^1/_4$	0	$^1/_2$	0.0166(8)
	Ba1 [b]	24k	0	0.2574(10)	0.4637(5)	0.0534(21)
	Ba2	2a	0	0	0	0.0203(6)
293(2)	Sn1/Ga1 [c]	24k	0	0.31220(7)	0.11848(6)	0.0185(3)
	Sn2/Ga2 [d]	16i	0.18425(5)	0.18425(5)	0.18425(5)	0.0192(4)
	Sn3/Ga3 [e]	6c	$^1/_4$	0	$^1/_2$	0.0195(7)

[a] U_{eq} is defined as one third of the trace of the orthogonalized U_{ij} tensor; [b] Off-set by cs. 0.4 Å from the ideal 6d position $(0\ ^1/_4\ ^1/_2)$. Occupancy is 25%; [c] Refined as statistically disordered Ga and Sn atoms in the ratio Ga:Sn = 23(2):77(2); [d] Refined as statistically disordered Ga and Sn atoms in the ratio Ga:Sn = 31(2): 69(2); [e] Refined as statistically disordered Ga and Sn atoms in the ratio Ga:Sn = 67(2):33(2).

Figure 2. Crystal structures of $Ba_8Ga_{14.5}Sn_{31.5(4)}$ (type-I, *left*) and $Ba_8Ga_{13.2}Sn_{32.8(3)}$ (type-VIII, *right*). Ba atoms residing in the $(Ga,Sn)_{20}$ cages (clathrate type-I) and the augmented $(Ga,Sn)_{20+3}$ cages (clathrate type-VIII) are drawn as light blue spheres, while the Ba atoms residing in the $(Ga,Sn)_{24}$ tetrakaidecahedra (clathrate type-I only) are drawn as red spheres. The empty cubic voids in the clathrate type-VIII are shown in yellow.
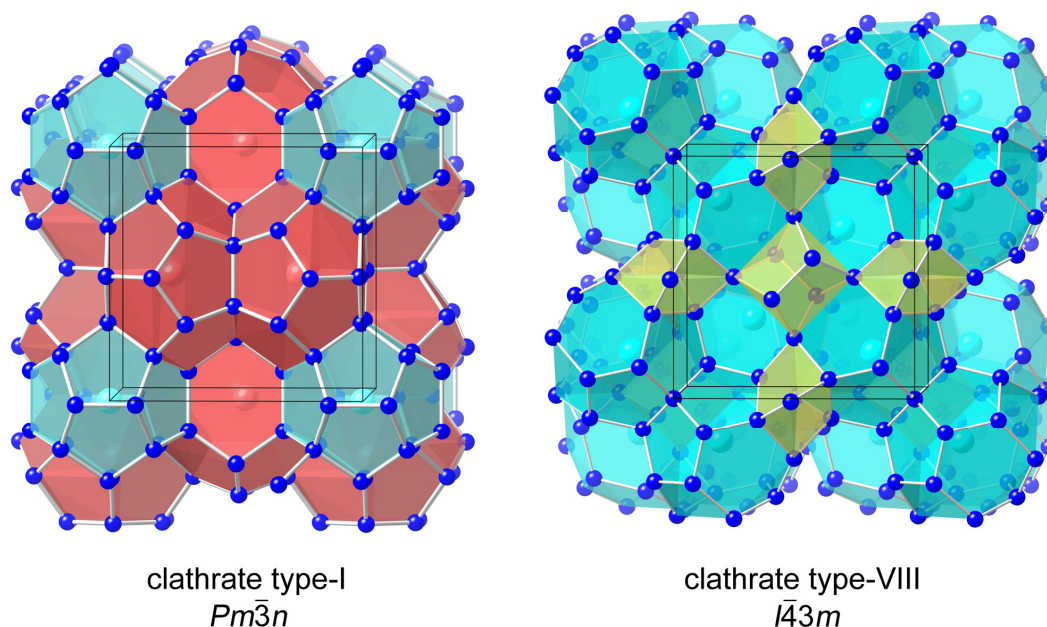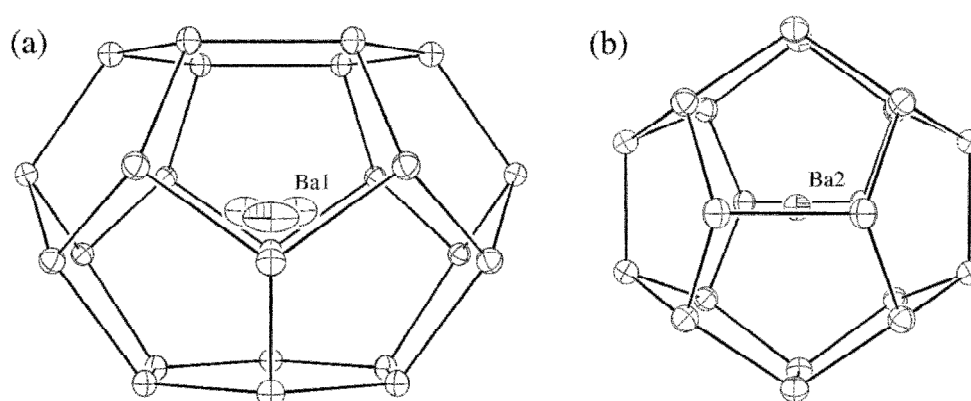

clathrate type-I
$Pm\bar{3}n$

clathrate type-VIII
$I\bar{4}3m$

Figure 3. Representations with anisotropic displacement parameters of: (**a**) the Ba1 atom at the 24*k* site (off-set from center of the $(Ga,Sn)_{24}$ tetrakaidecahedra); and (**b**) the Ba2 atom at the 2*a* site (center of the $(Ga,Sn)_{20}$ pentagonal dodecahedra). Thermal ellipsoids are drawn at the 95% probability level.

The $(Ga,Sn)_{24}$ tetrakaidecahedra host the Ba1 atoms, while the $(Ga,Sn)_{20}$ polyhedra encapsulate the Ba2 atoms (site 2*a*). The former reside not in the center of the cage (corresponding to site 6*d*), but are displaced by almost 0.4 Å to a 24*k* site (Figure 3). The 4-times greater multiplicity of the "off-center" position requires the Ba1 atom to be with a 25% occupation. Introducing positional disorder here is necessary because the anisotropic displacement parameter (ADP) of Ba1 is abnormally elongated if the

electron density is not modeled as smeared around the center of the cage (Figure 3). Such anisotropy and large thermal ellipsoids of the alkaline-earth metal located in the tetrakaidecahedra is well documented in the literature, not only for $Ba_8Ga_{16.8}Sn_{29.2}$ [11], but also for other type-I clathrates like $Ba_8Ga_{16-x}Ge_{30+x}$ [14,29], $Sr_8Ga_{16}Ge_{30}$ [30], $Ba_8Cd_xGe_{43-5x/8}\square_{3-3x/8}$ ($0 < x < 8$) [31], and $Ba_8Zn_xGe_{46-x-y}\square_y$ ($2 < x < 8$) [32].

From temperature dependent X-ray diffraction experiments carried out for a single-crystal of $Ba_8Ga_{14.5}Sn_{31.5(4)}$ (Table 2), we see a nearly linear increase of the lattice parameter from $a = 11.6588(8)$ Å at 100 K to $a = 11.6800(12)$ Å at room temperature. This yields a coefficient of linear thermal expansion $\beta = 9.6 \times 10^{-6}$ K^{-1}, which is comparable to many metals and alloys. Refinements of the anisotropic displacement parameters of all atoms and plotting the ADP values as a function of temperature is also instructive—the above described disorder at the Ba1 site can be clearly seen in Figure 4. The "jump" between 175 and 200 K is not understood as of yet, and might indicate the onset of an order-disorder transition, although the refinements at the six different temperatures agree well with the presented model. Such dynamic disorder has been previously dubbed "a rattling motion", which can be described by the Einstein oscillator model. Thereby, the temperature dependence of the Debye-Waller factors (assuming the rattling atoms to be harmonic oscillators exhibiting characteristic localized vibration frequency) can be given as $U_{iso} = k_BT/K = h^2T/(4\pi^2mk_B\Theta_E^2)$, where U_{iso} is the slope of the isotropic mean-square displacement; k_B is Boltzmann constant; T is temperature; K is the spring temperature of the oscillator, h is Planck's constant; m is the mass of the rattling atom; and Θ_E is the Einstein temperature [2]. The ADP data (Table 4) can be used to estimate the Einstein temperature of these atoms. This estimation results in $\Theta_E = 47$ K at 293 K for $Ba_8Ga_{14.5}Sn_{31.5}$. *Suekuni et al.* reported an Einstein temperature of $\Theta_E = 60$ K at 300 K for $Ba_8Ga_{15.8}Sn_{30.2}$ [13]. From this analysis it appears that the Ba atoms behave as normal "rattlers", even though we cannot ascertain from the ADP alone whether this corresponds to a static displacement or to some dynamic motion between the four off-center sites and the center of the cage.

Figure 4. Temperature dependence of the isotropic (**a**) and anisotropic displacement parameters (**b**) for $Ba_8Ga_{14.5}Sn_{31.5(4)}$ (clathrate type-I) in the interval 100–293 K.
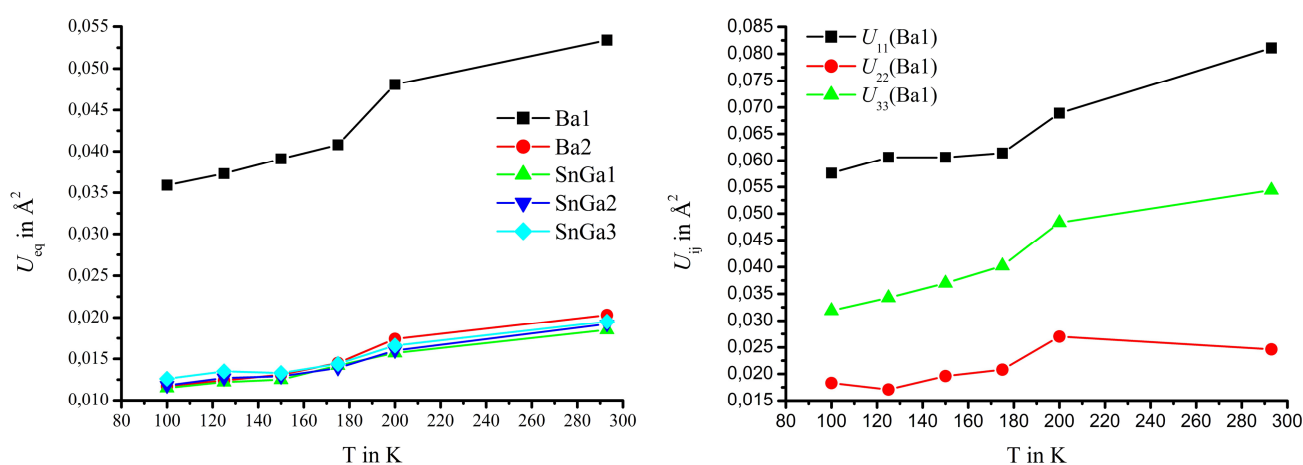
Table 4. Anisotropic displacement parameters (U_{ij}) for $Ba_8Ga_{14.5}Sn_{31.5(4)}$ (clathrate type-I) at variable temperature.

Atom	U_{11} (Å^2)	U_{22} (Å^2)	U_{33} (Å^2)	U_{23} (Å^2)	U_{13} (Å^2)	U_{12} (Å^2)
			100(2) K			
Ba1	0.0576(25)	0.0183(15)	0.0319(17)	0.0056(33)	0	0
Ba2	0.0117(5)	$= U_{11}$	$= U_{11}$	0	0	0
Sn1/Ga1	0.0133(4)	0.0108(4)	0.0115(4)	–0.0010(3)	0	0
Sn2/Ga2	0.0118(3)	$= U_{11}$	$= U_{11}$	0.0001(2)	$= U_{23}$	$= U_{23}$
Sn3/Ga3	0.0126(10)	0.0126(7)	$= U_{22}$	0	0	0
			125(2) K			
Ba1	0.0606(31)	0.0171(20)	0.0343(20)	0.0016(30)	0	0
Ba2	0.0124(6)	$= U_{11}$	$= U_{11}$	0	0	0
Sn1/Ga1	0.0145(4)	0.0110(4)	0.0112(4)	0.0006(3)	0	0
Sn2/Ga2	0.0127(3)	$= U_{11}$	$= U_{11}$	0.0001(2)	$= U_{23}$	$= U_{23}$
Sn3/Ga3	0.0136(10)	0.0134(8)	$= U_{22}$	0	0	0
			150(2) K			
Ba1	0.0606(38)	0.0196(38)	0.0370(25)	0.0038(50)	0	0
Ba2	0.0131(7)	$= U_{11}$	$= U_{11}$	0	0	0
Sn1/Ga1	0.0149(5)	0.0114(5)	0.0113(5)	0.0004(4)	0	0
Sn2/Ga2	0.0129(3)	$= U_{11}$	$= U_{11}$	0.0000(3)	$= U_{23}$	$= U_{23}$
Sn3/Ga3	0.0134(13)	0.0132(9)	$= U_{22}$	0	0	0
			175(2) K			
Ba1	0.0614(31)	0.0208(21)	0.0402(21)	0.0012(34)	0	0
Ba2	0.0145(6)	$= U_{11}$	$= U_{11}$	0	0	0
Sn1/Ga1	0.0165(5)	0.0132(4)	0.0130(4)	0.0009(3)	0	0
Sn2/Ga2	0.0139(3)	$= U_{11}$	$= U_{11}$	0.0001(2)	$= U_{23}$	$= U_{23}$
Sn3/Ga3	0.0151(10)	0.0140(7)	$= U_{22}$	0	0	0
			200(2) K			
Ba1	0.0689(42)	0.0270(25)	0.0483(30)	0.0043(60)	0	0
Ba2	0.0174(7)	$= U_{11}$	$= U_{11}$	0	0	0
Sn1/Ga1	0.0175(5)	0.0151(5)	0.0146(5)	0.0007(4)	0	0
Sn2/Ga2	0.0160(4)	$= U_{11}$	$= U_{11}$	0.0003(3)	$= U_{23}$	$= U_{23}$
Sn3/Ga3	0.0165(13)	0.0166(9)	$= U_{22}$	0	0	0
			293(2) K			
Ba1	0.0811(47)	0.0246(31)	0.0544(30)	0.0063(30)	0	0
Ba2	0.0203(6)	$= U_{11}$	$= U_{11}$	0	0	0
Sn1/Ga1	0.0214(5)	0.0175(5)	0.0166(4)	0.0012(3)	0	0
Sn2/Ga2	0.0192(4)	$= U_{11}$	$= U_{11}$	0.0007(2)	$= U_{23}$	$= U_{23}$
Sn3/Ga3	0.0191(11)	0.0147(8)	$= U_{22}$	0	0	0

2.3. Crystal Chemistry of Clathrate type-VIII

$Ba_8Ga_{13.2}Sn_{32.8(3)}$ with type-VIII structure crystallizes in the cubic space group $I\bar{4}3m$ (no. 217, *Pearson* symbol *cI*54; Table 1) with a periodicity constant $a = 11.5843(7)$ Å at room temperature. Notice that the unit cell parameters for type-I and type-VIII clathrates are very close, although the

former is around 0.1 Å longer than the latter. Here, we also observe the unexpected elongation of the unit cells for the Ga-richer $Ba_8Ga_{17.4}Sn_{28.6}$ (a = 11.5945(12) Å) [13] and $Ba_8Ga_{17.2}Sn_{28.8}$ (a = 11.5949(2) Å) [15] compared to the Sn-richer $Ba_8Ga_{13.2}Sn_{32.8(3)}$. The a-axis value and the refined composition are very well comparable to those in $Ba_8Ga_{16-x}Sn_{30+x}$ ($x \leq \pm 0.5$; a = 11.584(1)–11.589(1) Å) [12].

The crystal structure (Figure 2, *right*) can be viewed as a framework of face-shared distorted $(Ga,Sn)_{20}$ polyhedra, centered by the single Ba site (8*c*). These are bridged by an additional vertex resulting in $(Sn,Ga)_{20+3}$ cages ($6^36^35^35^3$), shown in light blue in Figure 2. The packing of the polyhedra is not space-filling, and small, empty cages of eight framework atoms are left behind (shown in yellow). There are four crystallographically unique sites and the Ga/Sn distribution on them varies greatly. The *Wyckoff* site 2*a* is exclusively occupied by Sn atoms, while the other three sites, 8*c*, 12*d* and 24*g*, are occupied by statistical mixtures of Ga and Sn atoms in the following ratios—Ga:Sn = 62:38 at the 8*c* site; Ga:Sn = 13:87 at the 12*d* site; and Ga:Sn = 28:72 at the 24*g* site, respectively (Table 5). A similar distribution on the four sites is found in $Ba_8Ga_{17.4}Sn_{28.6}$ by *Eisenmann et al.* (Sn amount: 2*a*: 100%, 8*c*: 34%, 12*d*: 65% and 24*g*: 67%) [13]. A largely different, yet unexplained, Ga/Sn distribution on all four sites can be found in the refinements of $Ba_8Ga_{17.2}Sn_{28.8}$ by *Carrillo-Cabrera et al.* [15] (Sn amount: 2*a*: 72%, 8*c*: 29%, 12*d*: 80% and 24*g*: 65%, respectively). Notice that the refined compositions are virtually identical in both cases, suggesting the preparative methods—convection heating *vs* induction heating and annealing—to be the reason for the observed differences.

Table 5. Atomic coordinates and equivalent isotropic displacement parameters $(U_{eq})^a$ for $Ba_8Ga_{13.2}Sn_{32.8(3)}$ (clathrate type-VIII), and $BaGa_{1.79}Sn_{4.21(2)}$.
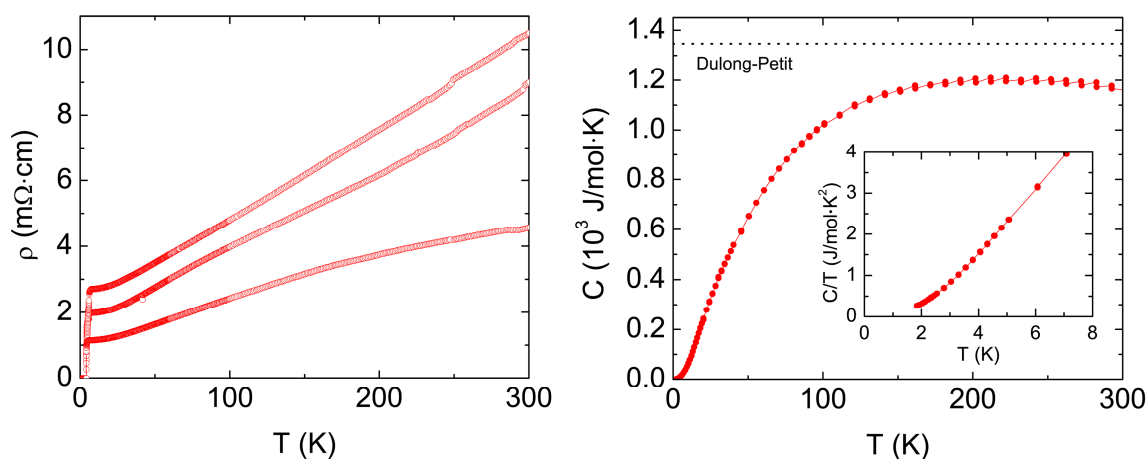
Atom	Site	x	y	z	Occupancy	U_{eq} (Å^2)
			$Ba_8Ga_{13.2}Sn_{32.8(3)}$			
Ba	8*c*	0.31496(6)	0.31496(6)	0.31496(6)		0.0444(4)
Sn1/Ga1	24*g*	0.08429(5)	0.08429(5)	0.35138(5)	72/28(1)	0.0198(3)
Sn2/Ga2	12*d*	$^1/_4$	$^1/_2$	0	87/13(1)	0.0241(4)
Sn3/Ga3	8*c*	0.13424(6)	0.13424(6)	0.13424(6)	38/62(2)	0.0186(5)
Sn4	2*a*	0	0	0		0.0193(5)
			$BaGa_{1.79}Sn_{4.21(2)}$			
Ba	4*c*	0	0.07183(6)	$^1/_4$		0.0119(2)
Sn1	8*f*	0	0.47132(5)	0.09526(5)		0.0119(2)
Sn2/Ga2	8*f*	0	0.07183(6)	0.15773(6)	50/50(1)	0.0087(3)
Sn3/Ga3	8*f*	0	0.25068(6)	0.04992(6)	60/40(1)	0.0118(3)

[a] U_{eq} is defined as one third of the trace of the orthogonalized U_{ij} tensor,

Detailed investigations of the thermoelectric properties, the electronic structure and carrier tuning of both type-I and type-VIII $Ba_8Ga_{16-x}Sn_{30+x}$ clathrates by virtue of optimizing the *p*- and *n*-type carriers can be found elsewhere [12,14,19,20]. We might just add here that utmost care should be exercised when synthesizing such compounds in large batches, as sample homogeneity and phase-purity could complicate the transport measurements. A testament to this conjecture is the resistivity measurements of three different batches of type-I $Ba_8Ga_{16-x}Sn_{30+x}$ clathrates, displayed in Figure 5. The three single-crystals are poor metals with room temperature resistivity between 4 and 10 mOhm·cm. These values are several orders of magnitude higher than the resistivities of normal

metals. As seen from the temperature dependence of $\rho(T)$, the resistivity decreases almost linearly with temperature, but the slopes are different, even though the samples have been prepared following the same synthetic procedure and are expected to be identical. Most likely, differences in the concentration of defects and impurities in the samples are the cause of such behaviour. At low temperature (below *ca.* 20 K), $\rho(T)$ in the three data sets rich plateaus, with residual resistivities occurring in the range from 1 and 3 mOhm·cm—obviously shows another sign of variations in the samples. Below *ca.* 5 K the resistivity of all samples drops to zero, which is indicative of superconducting transitions. Likely, the drops in the resistivities are not due to bulk superconductivity of the type-I $Ba_8Ga_{16-x}Sn_{30+x}$ clathrate, but to small amounts of Sn/Ga flux present in the samples, as confirmed by the heat capacity, illustrated for one of these samples in Figure 5 as well. The main panel in Figure 5 shows the heat capacity over the whole temperature range approaching the value predicted by the law of Dulong-Petit at high temperatures, as expected. In the inset C/T *vs* T is plotted in the temperature range around the superconducting plateaus found in the resistivity data. There are no indications of a transition, confirming that no bulk superconductivity is present in the samples.

Figure 5. Resistivity and specific heat as a function of temperature of single-crystalline type-I $Ba_8Ga_{16-x}Sn_{30+x}$ clathrate.
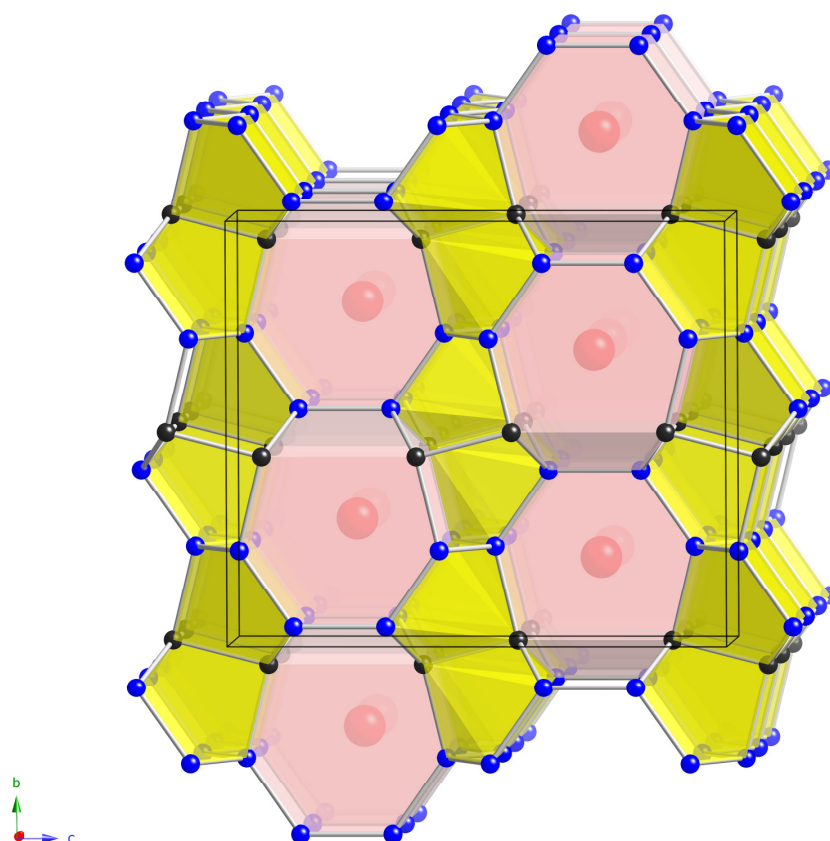

2.4. Crystal Chemistry of BaGa$_{1.79}$Sn$_{4.21(2)}$

The composition of the new ternary phase $BaGa_{2-x}Sn_{4+x}$ ($\equiv Ba_8Ga_{16-x}Sn_{32+x}$, $x \approx 1.6$) is very close to that of the above discussed $Ba_8Ga_{16-x}Sn_{30+x}$ clathrates, which could explain the difficulties obtaining this elusive compound as a single-phase material. $BaGa_{1.79}Sn_{4.21(2)}$ crystallizes in the orthorhombic space group *Cmcm* (no. 63, *Pearson* symbol *oS*28) with the cell parameters $a = 4.5383(6)$ Å, $b = 12.2486(16)$ Å and $c = 14.3747(19)$ Å and is isotypic to $EuGa_{2\pm x}Ge_{4\mp x}$ [16-18]. The zeolitic framework (Figure 6) is made up of large $(Ga,Sn)_{18}$ polyhedra with 7 faces ($6^26^26^18^2$), shown in red in the figure. They are face-shared to form layers running parallel to the (001) plane, which are separated by layers of fused $(Ga,Sn)_9$ cages. The large $(Ga,Sn)_{18}$ polyhedra encapsulate the Ba atoms (site 4*c*), while the smaller cages are empty. These slabs are arranged in an ABA'B' sequence along the crystallographic *c*-axis, where A'B' are received by reflection of AB as shown in Figure 6. Although this structure has been known for a decade and has been analyzed in great details [16-18], our

structural refinement is unprecedented because, for a first time, it provides the distribution of the Ga and Sn atoms on the framework sites—in all previous work on $EuGa_{2\pm x}Ge_{4\mp x}$ [16-18], the Ga/Ge occupancy has been assumed to be 1/3 Ga and 2/3 Ge on each site. In the case of $BaGa_{2-x}Sn_{4+x}$, the scattering factors for Ga and Sn are significantly different, enabling accurate structure refinements from X-ray single-crystal data. Hence, we ascertain that in agreement with the Ga/Sn occupancies in both type-I and type-VIII clathrates, the three framework sites in $BaGa_{2-x}Sn_{4+x}$ are not uniformly occupied by Ga and Sn. One of the three *Wyckoff* sites (all 8*f*), labeled Sn1 (Figure 6) is exclusively taken by Sn atoms, while the other two sites are occupied by Ga and Sn atoms almost without a preference (Sn amount of approx. 50% and 60%, respectively; Table 5).

Figure 6. Polyhedral view of the orthorhombic crystal structure of $BaGa_{2-x}Sn_{4+x}$. Ba atoms residing in the $(Ga,Sn)_{18}$ polyhedra are drawn as red spheres. The empty 9-atom voids are shown in yellow. Sn1 atoms (8*f* site, 100% occupancy by Sn) are shown as black spheres, while the remaining two framework sites with statistical mixtures of Sn/Ga atoms are represented as blue spheres, respectively.

The bond distances in $BaGa_{1.79}Sn_{4.21(2)}$ nicely follow the above-discussed site occupations, with the pure Sn sites exhibiting longest distances ($d_{Sn1-Sn1} = 2.828(1)$ Å) and the Ga/Sn2 sites exhibiting the shortest distances ($d_{Sn/Ga-Sn/Ga} = 2.653(2)–2.685(1)$ Å). The third framework site, Ga/Sn3 (with a Ga:Sn ratio of 3:2) has neighboring atoms at distance $d_{Sn-Sn/Ga} = 2.733(1)–2.780(1)$ Å, which are intermediate. The Ba–Sn1 distances are $d_{Ba-Sn} = 3.889(1)$ Å, slightly longer than the Ba–Ga/Sn2 and Ba–Ga/Sn3 contacts ($d_{Ba-Sn/Ga} = 3.692(1)–3.733(1)$ Å). These values are similar to the ones observed in the clathrate type-I ($d_{Sn/Ga-Sn/Ga} = 2.660(2)–2.730(1)$ Å, $d_{Ba-Sn/Ga} = 3.710(9)–4.129(3)$ Å) and the clathrate

type-VIII ($d_{\text{Sn/Ga–Sn/Ga}}$ = 2.645(1)–2.762(2) Å, $d_{\text{Ba–Sn/Ga}}$ = 3.626(2)–3.848(1) Å). The discussed bond lengths are also in good agreement with those reported for $Ba_8Ga_{17.4}Sn_{28.6}$ ($d_{\text{Sn/Ga–Sn/Ga}}$ = 2.642–2.764 Å, $d_{\text{Ba–Sn/Ga}}$ = 3.635–3.845 Å) [13], $Ba_8Ga_{17.2}Sn_{28.8}$ ($d_{\text{Sn/Ga–Sn/Ga}}$ = 2.649–2.766 Å, $d_{\text{Ba–Sn/Ga}}$ = 3.632–3.852 Å) [15], and as well as for other ternary compounds of Ba, Ga, and Sn, such as BaGaSn ($d_{\text{Sn/Ga–Sn/Ga}}$ = 2.676–2.677 Å; $d_{\text{Ba–Sn/Ga}}$ = 3.556–3.842 Å) [21]; $BaGa_{3.11}Sn_{0.89}$ ($d_{\text{Sn/Ga–Sn/Ga}}$ = 2.631–2.717 Å; $d_{\text{Ba–Sn/Ga}}$ = 3.549–3.962 Å) [22], $Ba_3Ga_{0.49}Sn_{4.51}$ ($d_{\text{Sn/Ga–Sn/Ga}}$ = 2.962–2.984 Å; $d_{\text{Ba–Sn}}$ = 3.500–3.881 Å) [23], and Ba_5Ga_5Sn ($d_{\text{Sn/Ga–Sn/Ga}}$ = 2.668–2.727 Å; $d_{\text{Ba–Sn}}$ = 3.461–4.099 Å) [24].

3. Experimental Section

All synthetic manipulations were carried out in an argon-filled glove box or under vacuum. In the syntheses we employed pure metallic elements, purchased from Alfa or Aldrich with purities greater than 99.9% (metal basis). Two methods were generally used—direct fusion of elements in sealed niobium containers and flux reactions with Ga or Sn as molten fluxes. The basic synthetic procedure for the former method was as follows: the elements were loaded in the desired stoichiometric ratios in niobium tubes, which were subsequently sealed using an arc-welder (under high purity Argon gas). The niobium tubes were then put in fused silica jackets, and flame-sealed under high vacuum. Melting the reaction mixtures was accomplished using suitable heating scheme in high temperature tube furnaces. The niobium tubes were then brought back in the glove box and opened. The basic synthetic procedure for the flux reactions was as follows: the elements were loaded in the desired molar ratios in 2 cm^3 alumina crucibles that were subsequently flame-sealed in evacuated fused silica tubes. The reaction mixtures were subjected to different heat treatments in high temperature muffle furnaces. Upon cooling to desired temperatures (above the melting point of the specific flux), the excess molten metal was removed by decantation. The silica tubes were then brought back in the glove box, crack-opened, and the crystals were isolated.

The new $BaGa_{1.79}Sn_{4.21(2)}$ compound was never obtained as a single phase product and always co-crystallized with type-I $Ba_8Ga_{14.5}Sn_{31.5(4)}$ clathrate, when Sn flux reaction were used. The optimized experiment involved a mixture Ba:Ga:Sn = 2:4:15, which was heated to 1000 °C (rate 10 °C/h), homogenized for 5 h, cooled to 450 °C (rate –300 °C/h), annealed for 28 h and cooled to 400 °C (rate –10 °C/h), where the excess Sn was removed. Clathrate type-I $Ba_8Ga_{16-x}Sn_{30+x}$ ($x \le \pm1.5$), in addition to the method above, could also be obtained by stoichiometric reactions Ba:Ga:Sn = 2:4:7.5. After sealing the mixtures in Nb tubes (jacketed in fused silica tubes), they were heated to 1000 °C (rate 10 °C/h), equilibrated for 5 h, cooled to 450 °C (rate –300 °C/h), annealed for 12 h and cooled to room temperature (rate –20 °C/h). The products from such reactions were identified by powder and single-crystal X-ray diffraction.

Clathrate type-VIII $Ba_8Ga_{13.2}Sn_{32.8(3)}$ is hard to obtain from stoichiometric reactions, but large (up to 4–5 mm) crystals can be readily grown from Ga/Sn flux reactions. The optimized experiment required the elements to be loaded in the Ba:Ga:Sn = 2.5:14:67 molar ratio. The samples were heated to 500 °C (rate 20 °C/h) and homogenized for 500 h. The flux was removed, after cooling to 400 °C (rate –5 °C/h).

The compositions of all synthesized materials were confirmed by EDX measurements (JEOL 7400F electron microscope equipped with an INCA-OXFORD energy-dispersive spectrometer).

X-ray powder diffraction patterns of all samples were taken at room temperature on a Rigaku MiniFlex powder diffractometer using Cu Kα radiation. Typical runs included θ–θ scans ($2\theta_{max} = 75°$) with the scan steps of 0.05° and 1 sec/step counting time. The JADE 6.5 software package [33] was used for data analysis. The intensities and the positions of the experimental observed peaks and those calculated from the crystal structures matched very well. Variable temperature *in-situ* X-ray powder diffraction patterns were collected on a Rigaku Ultima 3 powder diffractometer using Cu Kα radiation. The instrument was fitted with an Anton-Parr high-temperature furnace. Temperature was measured with a Pt-thermocouple.

Based on the results from powder XRD, the title compounds are presumed to be air-stable over extended periods (greater than 1 month).

Intensity data collections were carried out on a Bruker SMART CCD single-crystal X-ray diffractometer at variable temperatures. The source was graphite-monochromated Mo-Kα radiation ($\lambda = 0.71073$ Å). Suitable single crystals of each compound were selected in a glove box and cut under mineral oil to smaller dimensions (less than 0.1 mm). The *SMART* [34] and *SAINTplus* [35] programs were used for the data collection, integration and the global unit cell refinement from all data. Semi-empirical absorption correction was applied with *SADABS* [36]. The structures were refined to convergence by full matrix least-square methods on F^2, as implemented in *SHELXTL* [37]. All sites were refined with anisotropic displacement parameters. Other refined parameters included the scale factor, the atomic positions, and occupancy factors for the mixed positions. Selected details of the data collections and structure refinement parameters are summarized in Table 1 and 2. The atomic coordinates, equivalent isotropic and anisotropic displacement parameters are given in Tables 3–6, respectively. Additional details of the crystal structure investigations may be obtained from the Fachinformationszentrum Karlsruhe, D-76344 Eggenstein-Leopoldshafen, Germany (Fax: +49-7247-808-666, E-Mail: crysdata@fiz-karlsruhe.de) on quoting the depository numbers CSD-423287 for $Ba_8Ga_{14.5}Sn_{31.5(4)}$, CSD-423288 for $Ba_8Ga_{13.2}Sn_{32.8(3)}$, and CSD-423289 for $BaGa_{1.79}Sn_{4.21(2)}$, respectively.

We specifically note again that the contrast of the X-ray atomic scattering factor difference between Ga and Sn is large enough to refine mixed site occupations. In the refinements of the type-VIII clathrate $Ba_8Ga_{13.2}Sn_{32.8(3)}$, only Sn4 atoms were found at *Wyckoff* site 2*a*, while Sn and Ga atoms were located statistically disordered at 8*c*, 12*d* and 24*g* sites, respectively. In the type-I clathrate $Ba_8Ga_{14.5}Sn_{31.5(4)}$, all three sites 6*c*, 16*i* and 24*k* were statistically occupied by Sn and Ga atoms with a preference of Ga at 6*c* site. Additionally, Ba1 atoms were not located at the cage center position 6*d* but at *Wyckoff* site 24*k* with 25% occupation resulting in significant better anisotropic displacement parameters than for Ba1 atoms placed on 6*d*. The refinement of $BaGa_{1.79}Sn_{4.21(2)}$ leads to three possible sites, all 8*f*, for Sn and Ga. One of these sites, Sn1 is only occupied by tin atoms, while the other two sites take both kinds of atoms. The ADP's are normal (Table 5 and 6).

Four-probe measurements of the electrical resistivity and heat capacity measurements (thermal relaxation method) as a function of the temperature were carried out on a Quantum Design PPMS system in the interval 2 to 300 K with excitation current of 1 mA. The electrical resistivity was measured on at least two crystals from each batch to assure reproducibility. Polished single crystals were used to minimize geometric errors.

Table 6. Anisotropic displacement parameters (U_{ij}) for $BaGa_{1.79}Sn_{4.21(2)}$ and $Ba_8Ga_{13.2}Sn_{32.8(3)}$.

Atom	U_{11} ($\mathring{A}^2$)	U_{22} ($\mathring{A}^2$)	U_{33} ($\mathring{A}^2$)	U_{23} ($\mathring{A}^2$)	U_{13} ($\mathring{A}^2$)	U_{12} ($\mathring{A}^2$)
$Ba_8Ga_{13.2}Sn_{32.8(3)}$						
Ba	0.0444(4)	$= U_{11}$	$= U_{11}$	0.0105(3)	$= U_{23}$	$= U_{23}$
Sn1/Ga1	0.0211(3)	$= U_{11}$	0.0172(4)	0.0001(2)	$= U_{23}$	0.003(3)
Sn2/Ga2	0.190(5)	0.0266(4)	$= U_{22}$	0	0	0
Sn3/Ga3	0.0186(5)	$= U_{11}$	$= U_{11}$	0.0001(3)	$= U_{23}$	$= U_{23}$
Sn4	0.0193(5)	$= U_{11}$	$= U_{11}$	0	0	0
$BaGa_{1.79}Sn_{4.21(2)}$						
Ba	0.0070(4)	0.0131(4)	0.0155(5)	0	0	0
Sn1	0.0141(4)	0.0117(3)	0.0100(4)	0.0002(2)	0	0
Sn2/Ga2	0.0054(5)	0.0098(4)	0.0078(5)	0.0004(3)	0	0
Sn3/Ga3	0.0117(5)	00117(4)	0.0119(5)	0.0004(3)	0	0

4. Conclusions

Large single-crystals of the $Ba_8Ga_{14.5}Sn_{31.5(4)}$, which crystallizes with the clathrate-I structure (K_4Si_{23} structure type; cubic space group $Pm\bar{3}n$, *Pearson* symbol *cP*54) and $Ba_8Ga_{13.2}Sn_{32.8(3)}$, ($Eu_4Ga_8Ge_{15}$ structure type; cubic space group $I\bar{4}3m$, *Pearson* symbol *cI*54) were obtained using the flux method, following systematic investigations of the Ba–Ga–Sn ternary diagram. The new ternary phase $BaGa_{1.79}Sn_{4.21(2)}$ ($EuGa_2Ge_4$ structure type; orthorhombic space group *Cmcm*, *Pearson* symbol *oS*28) was also identified and structurally characterized. Our studies confirm that the control over whether type-I or type-VIII clathrates are realized is very subtle, with the heat treatments appearing to be the decisive factors. The next step in our investigations will be focused on application of chemical principles to find additional "tuning knobs", for example, by introducing mixtures of Al and Ga or Ga and In. These experiments will be analogous to the findings from the quaternary system Sr–Al–Ga–*Tt* (*Tt* = Si, Ge), where, by varying Al content in $Sr_8Al_xGa_{16-x}Si_{30}$, one can selectively prepare type-I ($x = 0$–7) or type-VIII ($x = 8$–13) [38,39]. The same idea has also been applied to $Sr_8Al_xGa_{16-x}Ge_{30}$ (type-I: $x = 4$, type-VIII: $x = 6, 8, 10$), although the Al-Ga solubility ranges are somewhat different [40]. Such studies are currently under way.

Acknowledgments

References and Notes

1. Nolas, G.S.; Cohn, J.L.; Slack, G.A.; Schjuman, S.B. Semiconducting Ge clathrates: Promising candidates for thermoelectric applications. *Appl. Phys. Lett.* **1998**, *73*, 178-180.
2. Sales, B.C.; Chakoumakos, B.C.; Mandrus, D.; Sharp, J.W. Atomic Displacement Parameters and the Lattice Thermal Conductivity of Clathrate-like Thermoelectric Compounds. *J. Solid State Chem.* **1999**, *146*, 528-532.

3. Christensen, M.; Johnson, S.; Iversen, B.B. Thermoelectric clathrates of type I. *Dalton Trans.* **2010**, *39*, 978-992.

4. The rationale here is based on the consideration that {14–p} extra electrons will be needed per idealized formula $A_8E_xTt_{46-x}$, where A is a n-valent guest metal, E is the heteroatom with group number p that substitutes a framework-building Tt-atom. Since $x = 8n/(14-p)$, the idealized compositions such as $A_8Tr_8Tt_{38}$ and $A_8E_4Tt_{42}$, $[AE]_8Tr_{16}Tt_{30}$ and $[AE]_8E_8Tt_{38}$, where AE = alkaline- or divalent rare-earth, Tr (Triel) = group 13 and E = group 12 elements, respectively, will be electronically balanced Zintl phases, *i.e.,* semiconducting materials.

5. Bobev, S.; Sevov, S.C. Synthesis and characterization of stable stoichiometric clathrates of silicon and germanium: $Cs_8Na_{16}Si_{136}$ and $Cs_8Na_{16}Ge_{136}$. *J. Amer. Chem. Soc.* **1999**, *121*, 3795-3796.

6. Bobev, S.; Sevov, S.C. Clathrates of group 14 with alkali metals: an exploration. *J. Solid State Chem.* **2000**, *153*, 92-105.

7. Bobev, S.; Meyers, J., Jr.; Fritsch, V.; Yamasaki, Y. Synthesis and structural characterization of novel clathrate-II compounds of silicon. *Proc. Int. Conf. Thermoelectr.* **2006**, *25*, 48-52.

8. Cros, C.; Pouchard, M.; Hagenmuller, P. Sur deux nouvelles structures du silicium et du germanium de type Clathrate. *Bull. Soc. Chim. Fr.* **1971**, *1971*, 379-386.

9. von Schnering, H.G.; Kröner, R.; Menke, H.; Peters, K.; Nesper, R. Crystal structure of the clathrates $Rb_8Ga_8Sn_{38}$, $Rb_8Ga_8Ge_{38}$ and $Rb_8Ga_8Si_{38}$. *Z. Kristallogr. NCS* **1998**, *213*, 677-678.

10. Paschen, S.; Carillo-Cabrera, W.; Bentien, A.; Tran, V.H.; Baenitz, M.; Grin, Yu.; Steglich, F. Structural, transport, magnetic, and thermal properties of $Eu_8Ga_{16}Ge_{30}$. *Phys. Rev.* **2001**, *B64*, 214404.

11. von Schnering, H.G.; Carillo-Cabrera, W.; Kröner, R.; Peters, E.-M.; Peters, K. Crystal structure of the clathrate β-$Ba_8Ga_{16}Sn_{30}$. *Z. Kristallogr. NCS* **1998**, *213*, 679-679.

12. Suekuni, K.; Avila, M.A.; Umeo, K.; Fukuoka, H.; Yamanaka, S.; Nakagawa, T.; Takabatake, T. Simultaneous structure and carrier tuning of dimorphic clathrate $Ba_8Ga_{16}Sn_{30}$. *Phys. Rev.* **2008**, *B77*, 235119.

13. Eisenmann, B.; Schäfer, H.; Zagler, R. Die Verbindungen $A_8B_{16}C_{30}$ (A = Sr, Ba; B = Al, Ga; C = Si, Ge, Sn) und ihre Käfigstrukturen. *J. Less-Common Met.* **1986**, *118*, 43-55.

14. Avila, M.A.; Suekuni, K.; Umeo, K.; Fukuoka, H.; Yamanaka, S.; Takabatake, T. Glasslike versus crystalline thermal conductivity in carrier-tuned $Ba_8Ga_{16}X_{30}$ clathrates (X = Ge, Sn). *Phys. Rev.* **2006**, *B74*, 125109.

15. Carrillo-Cabrera, W.; Cardoso Gil, R.H.; Tran, V.H.; Grin, Yu. Refinement of the crystal structure of $Ba_8Ga_{17.2}Sn_{28.8}$. *Z. Kristallogr. NCS* **2002**, *217*, 181-182.

16. Bryan, J.D.; Stucky, G.D. $Eu_4Ga_8Ge_{16}$: A New Four-Coordinate Clathrate Network. *Chem. Mater.* **2001**, *13*, 253-257.

17. Carrillo-Cabrera, W.; Paschen, S.; Grin, Yu. $EuGa_{2\pm x}Ge_{4\mp x}$: preparation, crystal chemistry and properties. *J. Alloys Compd.* **2002**, *333*, 4-12.

18. Christensen, M.; Bryan, J.D.; Birkedal, H.; Stucky, G.D.; Lebech, B.; Iversen, B.B. Crystal and magnetic structure of $Eu_4Ga_8Ge_{16}$. *Phys. Rev.* **2003**, *B68*, 174428.

19. Kono, Y.; Ohya, N.; Taguchi, T.; Suekuni, K.; Takabatake, T.; Yamamoto, S.; Akai, K. First-principles study of type-I and type-VIII $Ba_8Ga_{16}Sn_{30}$ clathrates. *J. Appl. Phys.* **2010**, *107*, 123720.

20. Mori, T.; Iwamoto, K.; Kushibiki, S.; Honda, H.; Matsumoto, H.; Toyota N.; Avila, M.A.; Suekuni, K.; Takabatake, T. Optical Conductivity Spectral Anomalies in the Off-Center Rattling System β-$Ba_8Ga_{16}Sn_{30}$. *Phys. Rev. Lett.* **2011**, *106*, 015501.

21. Evans, J.E.; Wu Yang; Kranak, V.F.; Newman, N.; Reller, A.; Garcia-Garcia, F.J.; Häussermann, U. Structural properties and superconductivity in the ternary intermetallic compounds MAB (M = Ca, Sr, Ba; A = Al, Ga, In; B = Si, Ge, Sn). *Phys. Rev.* **2009**, *B80*, 064514.

22. Tobash, P.H.; Yamasaki, Y.; Bobev, S. Gallium-tin mixing in $BaGa_{4-x}Sn_x$ [x = 0.89(2)] with the $BaAl_4$ structure type. *Acta Crystallogr.* **2007**, *63C*, i35-i37.

23. Dürr, I.; Schwarz, M.; Wendorff, M.; Röhr, C. Novel barium triel/tetrelides with the Pu_3Pd_5 structure type. *J. Alloys Compd.* **2010**, *494*, 62-71.

24. Guttsche, K.; Rosin, A.; Wendorff, M.; Röhr, C. $Ba_5(Al/Ga)_5(Sn/Pb)$: Neue Verbindungen an der Zintl-Grenze. *Z. Naturforsch.* **2006**, *61B*, 846-853.

25. Kröner, R.; Peters, K.; von Schnering, H.G.; Nesper, R. Crystal structure of the clathrate-II, $Ba_{16}Ga_{32}Sn_{104}$. *Z. Kristallogr. NCS* **1998**, *644*, 664-664.

26. Schäfer, M.C.; Yamasaki, Y.; Fritsch, V.; Bobev, S. Indium Doping in $BaSn_{3-x}In_x$ ($0 \leq x \leq 0.2$) with Ni_3Sn Structure. *Crystals* **2011**, *1*, 104-111.

27. Huo, D.; Sakata, T. Sasakawa, T.; Avila, M.A.; Tsubota M.; Iga, F.; Fukuoka, H. Yamanaka, S.; Aoyagi, S.; Takabatake, T. Structural, transport, and thermal properties of the single-crystalline type-VIII clathrate $Ba_8Ga_{16}Sn_{30}$. *Phys. Rev*. **2005**, *B71*, 075113.

28. Pauling, L.; Kamb, B. A revised set of values of single-bond radii derived from the observed interatomic distances in metals by correction for bond number and resonance energy (statistical theory of resonance of covalent bonds). *Proc. Nat. Acad. Sci. USA* **1986**, *83*, 3569-3571.

29. Christensen, M.; Juramyi, F.; Iversen, B.B. The rattler effect in thermoelectric clathrates studied by inelastic neutron scattering. *Physica B* **2006**, *385-586*, 505-507.

30. Chakoumakos, B.C.; Sales, B.C.; Mandrus, D.; Nolas, G.S. Structural disorder and thermal conductivity of the semiconducting clathrate $Sr_8Ga_{16}Ge_{30}$. *J. Alloys Compd.* **2000**, *296*, 80-86.

31. Melnychenko-Koblyuk, N.; Grytsiv, A.; Berger, St.; Kaldarar, H.; Michor, H.; Röhrbacher, F.; Royanian, F.; Bauer, E.; Rogl, P.; Schmid, H.; Giester, G. Ternary clathrates Ba–Cd–Ge: phase equilibria, crystal chemistry and physical properties. *J. Phys.: Condens. Matter* **2007**, *19*, 046203.

32. Melnychenko-Koblyuk, N.; Grytsiv, A.; Fornasarf, L.; Kaldarar, H.; Michor, H.; Röhrbacher, F.; Koza, M.; Royanian F.; Bauer, E.; Rogl, P.; Rotter, M.; Marabelli, F.; Devishvili, A.; Doerr, M.; Giester, G. Ternary clathrates Ba–Zn–Ge: phase equilibria, crystal chemistry and physical properties. *J. Phys.: Condens. Matter* **2007**, *19*, 216223.

33. *JADE*, Version 6.5; Materials Data, Inc.: Livermore, CA, USA, 2003.

34. *SMART NT*, Version 5.63; Bruker Analytical X-ray Systems Inc.: Madison, WI, USA, 2003.

35. *SAINT NT*, Version 6.45; Bruker Analytical X-ray Systems Inc.: Madison, WI, USA, 2003.

36. *SADABS NT*, Version 2.10; Bruker Analytical X-ray Systems Inc.: Madison, WI, USA, 2001.

37. *SHELXTL*, Version 6.12; Bruker Analytical X-ray Systems Inc.: Madison, WI, USA, 2001.

38. Kishimoto, K.; Ikeda, N.; Akai, K.; Koyanagi, T. Synthesis and thermoelectric properties of silicon clathrates $Sr_8Al_xGa_{16-x}Si_{30}$ with the type-I and type-VIII structures. *Appl. Phys. Express* **2008**, *1*, 031201.

39. Shimizu, H.; Takeuchi, Y.; Kume, T.; Sasaki, S.; Kishimoto, K.; Ikeda, N.; Koyanagi, T. Raman spectroscopy of type-I and type-VIII silicon clathrate alloys $Sr_8Al_xGa_{16-x}Si_{30}$. *J. Alloys Compd.* **2009**, *487*, 47-51.

40. Sasaki, S.; Kishimoto, K.; Koyanagi, T.; Asada, H.; Akai, K. Synthesis and thermoelectric properties of the type-VIII germanium clathrates $Sr_8Al_xGa_yGe_{46-x-y}$. *J. Appl. Phys.* **2009**, *105*, 073702.